Tropical tree growth driven by dry-season climate variability

Pieter A. ZUIDEMA[1], Flurin BABST[2,3], Peter GROENENDIJK[4], Valerie TROUET[3], Abrham ABIYU[5], Rodolfo ACUÑA-SOTO[6], Eduardo ADENESKY-FILHO[7], Raquel ALFARO-SÁNCHEZ[8], José Roberto Vieira ARAGÃO[4], Gabriel Assis-PEREIRA[9,10], Xue BAI[11], Ana Carolina BARBOSA[10], Giovanna BATTIPAGLIA[12], Hans BEECKMAN[13], Paulo Cesar BOTOSSO[14], Tim BRADLEY[15], Achim BRÄUNING[16], Roel BRIENEN[17], Brendan M. BUCKLEY[18], J. Julio CAMARERO[19], Ana CARVALHO[20], Gregório CECCANTINI[21], Librado R. CENTENO-ERGUERA[22], Julián CERANO-PAREDES[22], Álvaro Agustín CHÁVEZ-DURÁN[23], Bruno Barçante Ladvocat CINTRA[21], Malcolm K. CLEAVELAND[24], Camille COURALET[13], Rosanne D'ARRIGO[18], Jorge Ignacio DEL VALLE[25], Oliver DÜNISCH[26], Brian J. ENQUIST[27,28], Karin ESEMANN-QUADROS[29], Zewdu ESHETU[30], Ze-Xin FAN[11], M. Eugenia FERRERO[31,32], Esther FICHTLER[33], Claudia FONTANA[9], Kainana S. FRANCISCO[34], Aster GEBREKIRSTOS[35], Emanuel GLOOR[17], Daniela GRANATO-SOUZA[24], Kristof HANECA[36], Grant Logan HARLEY[37], Ingo HEINRICH[38,39,40], Gerd HELLE[40], Janet G. INGA[32], Mahmuda ISLAM[16,41], Yu-mei JIANG[42], J. Mark KAIB[43], Zakia Hassan KHAMISI[3], Marcin KOPROWSKI[44], Bart KRUIJT[45], Eva LAYME[46], Rik LEEMANS[47], A. Joshua LEFFLER[48], Claudio Sergio LISI[49], Neil J. LOADER[50], Giuliano Maselli LOCOSSELLI[21,51], Lidio LOPEZ[31], María I. LÓPEZ-HERNÁNDEZ[52], José Luís Penetra Cerveira LOUSADA[53], Hooz A. MENDIVELSO[54], Mulugeta MOKRIA[16,35], Eddy MOORS[55,56], Cristina NABAIS[20], Justine NGOMA[57], Francisco de Carvalho NOGUEIRA JÚNIOR[58], Juliano Morales OLIVEIRA[59], Gabriela Morais OLMEDO[59], Mariana Alves PAGOTTO[49], Shankar PANTHI[11], Gonzalo PÉREZ-DE-LIS[60], Darwin PUCHA-COFREP[61], Nathsuda PUMIJUMNONG[62], Mizanur RAHMAN[16,41], Jorge Andres RAMIREZ[63], Edilson Jimmy REQUENA-ROJAS[32], Adauto de Souza RIBEIRO[49], Iain ROBERTSON[50], Fidel Alejandro ROIG[31,64], Ernesto Alonso RUBIO-CAMACHO[65], Ute SASS-KLAASSEN[1], Jochen

SCHÖNGART[66], Paul R. SHEPPARD[3], Franziska SLOTTA[67], James H. SPEER[68], Matthew D. THERRELL[69], Benjamin TOIRAMBE[13], Mario TOMAZELLO-FILHO[9], Max C.A. TORBENSON[70], Ramzi TOUCHAN[3], Alejandro VENEGAS-GONZÁLEZ[64], Ricardo VILLALBA[31], Jose VILLANUEVA-DIAZ[22], Royd VINYA[71], Mart VLAM[72], Tommy WILS[73], Zhe-Kun ZHOU[11]

[1]Forest Ecology & Forest Management Group, Wageningen University, Wageningen, The Netherlands. [2]School of Natural Resources and the Environment, University of Arizona, Tucson, AZ, USA. [3]Laboratory of Tree-Ring Research, University of Arizona, Tucson, USA. [4]Department of Plant Biology, Institute of Biology, P.O. Box: 6109, University of Campinas (UNICAMP), 13083-970, Campinas, SP, Brazil. [5]World Agroforestry Centre (ICRAF), C/O ILRI Campus, Gurd Shola, P.O. Box 5689, Addis Ababa, Ethiopia. [6]Department of Microbiology and Parasitology, Universidad Nacional Autónoma de México, Mexico City, Mexico. [7]Laboratory of Protection and Forest Management, Department of Forest Engineering, Universidade Regional de Blumenau, R. São Paulo 3366, Itoupava Seca, Santa Catarina, 89030-000, Brazil. [8]Department of Biology, Wilfrid Laurier University, 75 University Avenue W, Waterloo, ON, N2L 3C5, Canada. [9]Forest Science Department, Luiz de Queiroz College of Agriculture, University of São Paulo, Av. Pádua Dias 11, Piracicaba - SP, 13418-900, Brazil. [10]Tree-Ring Laboratory, Forest Sciences Department, Federal University of Lavras, 37200-000, Lavras, MG, Brazil. [11]CAS Key Laboratory of Tropical Forest Ecology, Xishuangbanna Tropical Botanical Garden of the Chinese Academy of Sciences, Mengla, Yunnan, China. [12]University of Campania "L. Vanvitelli", Department of Environmental, Biological and Pharmaceutical Sciences and Technologies, via Vivaldi 43, 81100, Caserta, Italy. [13]Service of Wood Biology, Royal Museum for Central Africa, Leuvense steenweg 13, 3080 Tervuren Belgium. [14]Brazilian Agricultural Research Corporation (Embrapa), Embrapa

Forestry, Estrada da Ribeira - Km 111, 83411-000, Colombo, PR, Brazil. [15]U.S. Department of Agriculture, Forest Service, NWCG Member Agency. [16]Institute of Geography, Friedrich-Alexander-University Erlangen-Nuremberg, Wetterkreuz 15, 91058, Erlangen, Germany. [17]School of Geography, University of Leeds, Leeds, LS2 9JT, UK. [18]Lamont-Doherty Earth Observatory, Columbia University, Palisades, New York, USA. [19]Instituto Pirenaico de Ecología (IPE-CSIC), E-50192 Zaragoza, Spain. [20]Centre for Functional Ecology, Department of Life Sciences, Faculty of Sciences and Technology, University of Coimbra, Portugal. [21]Department of Botany, Institute of Biosciences, University of São Paulo, R. do Matão, 277, São Paulo, 05508-090, Brazil. [22]Instituto Nacional de Investigaciones Forestales, Agrícolas y Pecuarias (INIFAP), Margen Derecho del Canal del Sacramento Km 6.5, C.P. 35140, Gómez Palacio, Durango, México. [23]Instituto Nacional de Investigaciones Forestales, Agrícolas y Pecuarias (INIFAP), Campo Experimental Centro - Altos de Jalisco, Av. Biodiversidad 2470, C.P. 47600, Tepatitlán de Morelos, Jalisco, México. [24]Department of Geosciences, 267 Gearhart Hall, University of Arkansas, Fayetteville, AR 72701. [25]Departament of Forest Sciences, Universidad Nacional de Colombia - Sede Medellín. [26]Master School for Carpentry and Cabinetmaking, Gleusdorfer Str. 14, D-96106 Ebern, Germany. [27]Department of Ecology and Evolutionary Biology, University of Arizona, Tucson, AZ 85721, USA. [28]Santa Fe Institute, 1399 Hyde Park Rd., Santa Fe, NM 87501, USA. [29]Department of Biological Sciences, University of Joinville Region - UNIVILLE, Joinville, SC, Brazil. [30]Addis Ababa University, College of Life Science, Climate Science Center and Department of Earth Science, Addis Ababa, Ethiopia. [31]Departamento de Dendrocronología e Historia Ambiental, IANIGLA, CCT-CONICET-Mendoza, Av. Ruiz Leal s/n, Parque Gral. San Martín, CC 330, CP 5500, Mendoza, Argentina. [32]Laboratorio de Dendrocronología, Universidad Continental. Av. San Carlos 1980, Huancayo, Perú. [33]Department of Crop

71 Sciences, Tropical Plant Production and Agricultural Systems Modelling, Göttingen
72 University, Grisebachstrasse 6, Göttingen, 37077, Germany. [34]USDA Forest Service, Pacific
73 Southwest Research Station, Institute of Pacific Islands Forestry, Hilo, HI, USA. [35]World
74 Agroforestry Centre (ICRAF), United Nations Avenue, P.O. Box 30677-00100, Nairobi,
75 Kenya. [36]Flanders Heritage Agency, Havenlaan 88 box 5, 1000 Brussels,
76 Belgium. [37]Department of Geography and Geological Sciences, University of Idaho, Moscow,
77 ID, USA. [38]German Archaeological Institute DAI, 14195, Berlin, Germany. [39]Geography
78 Department, Humboldt-University Berlin, 12489, Berlin, Germany. [40]GFZ German Research
79 Centre for Geosciences, 14473, Potsdam, Germany. [41]Department of Forestry and
80 Environmental Science, Shahjalal University of Science and Technology, Sylhet 3114,
81 Bangladesh. [42]Faculty of Forestry and Wood Sciences, Czech University of Life Sciences
82 Prague, Prague, Czech Republic. [43]U.S. Fish and Wildlife Service, Region 2, 500 Gold Ave. SW,
83 PO BOX 1306, Albuquerque, NM 87103, USA. [44]Department of Ecology and Biogeography,
84 Faculty of Biology and Environment Protection, Nicolaus Copernicus University, Lwowska 1,
85 87-100, Toruń, Poland. [45]Water Systems and Global Change Group, Wageningen University
86 and Research, P.O. Box 47,6700AA Wageningen, the Netherlands. [46]Instituto Nacional de
87 Innovación Agraria, Programa Nacional de Investigación Forestal, Hualahoyo km 8,
88 Huancayo, Perú. [47]Environmental Systems Analysis Group, Wageningen University and
89 Research, P.O. Box 47, 6700AA Wageningen, the Netherlands. [48]Department of Natural
90 Resource Management, South Dakota State University, Brookings, SD, USA. [49]Laboratory of
91 Plant Anatomy and Dendrochronology, Department of Biology, Universidade Federal de
92 Sergipe, Av. Marechal Rondon s/n, Rosa Elze, São Cristóvão, Sergipe, 49100-000,
93 Brazil. [50]Department of Geography, Swansea University, Singleton Campus, Swansea, SA2
94 8PP, UK. [51]Institute of Botany, Ecology Group, Av. Miguel Stefano 3687, São Paulo 04301-

902, Brazil. [52]Departamento Forestal, Universidad Autónoma Agraria Antonio Narro, Calzada Antonio Narro No 1923, Buenavista, CP 25315, Saltillo, Coahuila, Mexico. [53]Department of Forestry Sciences and Landscape (CIFAP), University of Trás-os-Montes and Alto Douro, Quinta de Prados, 5000-801, Vila Real, Portugal. [54]Escuela de Ciencias Biológicas, Universidad Pedagógica y Tecnológica de Colombia (UPTC), Avenida Central del Norte 39-115, Tunja, Colombia. [55]IHE Delft, P.O. Box 3015, 2601 DA Delft, The Netherlands. [56]VU University Amsterdam, De Boelelaan 1085, 1081 HV Amsterdam, the Netherlands. [57]Department of Biomaterials Science and Technology, School of Natural Resources, The Copperbelt University, P.O. Box 21692, Kitwe, Zambia. [58]Laboratory of Ecology and Dendrology of the Federal Institute of Sergipe, Rodovia BR-101, Km 96, povoado Quissamã, São Cristovão, Sergipe, 49100-000, Brazil. [59]Laboratory of Plant Ecology, Universidade do Vale do Rio dos Sinos (UNISINOS), Av. Unisinos, 950, Cristo Rei, São Leopoldo, RS, 93022-750, Brazil. [60]Departamento de Botánica, Universidade de Santiago de Compostela, EPSE, Campus Terra, 27002 Lugo, Spain. [61]Laboratorio de Dendrocronología, Carrera de Ingeniería Forestal, Universidad Nacional de Loja, 110101 Loja, Ecuador. [62]Faculty of Environment and Resource studies, Mahidol University, 999 Phutthamonthon Rd4, Salaya, Phutthamonthon, Nakhon Pathom 73170, Thailand. [63]Facultad de Ciencias Agrarias, Universidad del Cauca, Popayán, Colombia. [64]Hémera Centro de Observación de la Tierra, Escuela de Ingeniería Forestal, Facultad de Ciencias, Universidad Mayor, Santiago, Chile. [65]Instituto Nacional de Investigaciones Forestales, Agrícolas y Pecuarias (INIFAP), Centro de Investigación Regional Pacífico Centro - Campo Experimental, Centro Altos de Jalisco, Jalisco, México. [66]National Institute for Amazon Research, Av. André Araújo, 2.936, Petrópolis, CEP 69.067-375, Manaus, Amazonas, Brazil. [67]Department of Earth Sciences, Freie Universität Berlin, Malteserstraße 74-100, 12249 Berlin, Germany. [68]Department of Earth and Environmental

Systems, Indiana State University, Science 159E, Terre Haute, IN, 47809 USA. [69]Department of Geography, University of Alabama, Tuscaloosa, AL, USA. [70]Department of Civil, Environmental and Geodetic Engineering, The Ohio State University, Columbus, OH, 43210, United States. [71]Department of Plant and Environmental Sciences, School of Natural Resources, The Copperbelt University, P.O. Box 21692, Kitwe, Zambia. [72]Forest and Nature Management, Van Hall Larenstein Univerisity of Applied Sciences, Velp, The Netherlands. [73]School of Teacher Training for Secondary Education Tilburg, Fontys University of Applied Sciences, Tilburg, The Netherlands.

Corresponding author: Pieter A. Zuidema, e-mail: Pieter.Zuidema@wur.nl

Interannual variability in the global land carbon sink is strongly related to variations in tropical temperature and rainfall. This association suggests an important role for moisture-driven fluctuations in tropical vegetation productivity, but empirical evidence to quantify the responsible ecological processes is missing. Such evidence can be obtained from tree-ring data that quantify variability in a major vegetation productivity component: woody biomass growth. Here we compile a pantropical tree-ring network to show that annual woody biomass growth increases primarily with dry-season precipitation and decreases with dry-season maximum temperature. The strength of these dry-season climate responses varies among sites, as reflected in four robust and distinct climate response groups of tropical tree growth derived from clustering. Using cluster and regression analyses, we find that observed dry-season climate responses are amplified in regions that are drier, hotter, and more climatically variable. These amplification patterns suggest that projected global warming will likely aggravate drought-induced declines in annual tropical vegetation productivity. Our study reveals a previously underappreciated role of dry-season climate variability in driving the dynamics of tropical vegetation productivity, and consequently influencing the land carbon sink.

Tropical and subtropical ecosystems are primarily responsible for the large interannual variability in the global carbon land sink[1-4]. In cooler and wetter years in the tropics, carbon uptake by tropical vegetation is large and increases the global land sink, whereas warmer and drier years reduce this sink[5-7] or flip it into a carbon source[8]. The response of tropical vegetation productivity to variability in moisture availability likely contributes to these emergent global patterns[6]. A better understanding of the global land sink variability therefore requires quantifying the effect of climatic variation on tropical vegetation productivity. Yet, the sensitivity of key components of tropical vegetation productivity, such

as woody biomass growth, to climate variability is poorly understood. Direct, long-term, and temporally highly resolved measurements of these components are needed to reconstruct[2], simulate[9,10], and forecast the carbon land sink[11,12].

Here, we evaluate the climate responses of woody biomass growth throughout the global tropics (here defined as 30°N-30°S, including subtropics). We focus on woody biomass growth in tree stems, which constitutes a significant share of net productivity of tropical vegetation at local[13,14] to continental scales[15,16], contributes to the main long-term carbon reservoir in tropical biomass[17], and determines the success of forest-based natural climate solutions[18]. Using an unprecedented compilation of tropical tree-ring data, we test three hypotheses on the association between climate and annual woody biomass growth of trees (hereafter 'tree growth') across tropical climate zones that vary in temperature and precipitation. (1) We expect opposite associations of tree growth with precipitation (positive) and temperature (negative), consistent with those observed for the land sink[5,6]. (2) We expect the magnitude of these associations to peak in the wet season, when photosynthesis[19] and woody biomass growth[20] in tropical vegetation are typically highest. (3) Finally, we expect climate-growth associations to amplify with site aridity, because semi-arid regions exhibit stronger climatic variability[1] and contribute more to interannual variability in the land sink[1,3,4,21]. Hereafter, we will refer to associations between climate and tree growth as 'climate responses'.

We established a network of 415 tree-ring chronologies (i.e., time series of absolutely dated, population-level average ring width) compiled from tropical and subtropical latitudes (Extended Data Fig. 1). From this network, we selected 347 chronologies that fulfilled quality criteria of sample size, chronology robustness and length, and that covered recent decades.

The chronologies are derived from 99 tree species on five continents and were obtained from co-authors (n = 112 chronologies) and the International Tree-Ring Data Bank (ITRDB; n = 235).

To facilitate comparative analyses of tree climate responses across the network, we re-developed standardized ring-width index (RWI) chronologies using a single detrending method. We then assessed climate associations by relating the most recent 50 years of all RWI chronologies to gridded climate data (Extended Data Table 1). We chose to evaluate climate associations to precipitation (P) and maximum temperature (T_{max}) instead of commonly used drought indices, because these climate data are directly measured, available for multiple decades, and because T_{max} is a strong driver of tropical woody biomass growth[22].

We tested our first two hypotheses using two complementary approaches. First, to detect common modes of climate response across the network, regardless of biogeographic region, we performed a self-organizing maps (SOM)[23] cluster analysis based on RWI responses to monthly P and T_{max} over a 2-year period during and prior to the year of ring formation. This approach allows for detecting idiosyncratic and lagged responses of tree growth to monthly climatic conditions[24]. We present the results based on a 2x2 SOM-grid, which resulted in four groups of climate response. Second, to evaluate the relative influence of T_{max} and P on tree growth during the wet (P>100 mm/mo)[46] and dry season (P<100 mm/mo; preceding ring formation), we conducted a multiple linear regression analysis of RWI for each chronology. This more restrictive analysis included only seasonally significant (p<0.05) and additive effects of the two climatic variables during a 1-year period. For both approaches, we tested hypothesis 3 by associating climate responses to ambient hydroclimatic conditions.

199

200 **Network representativeness**

201 Our network covers a large portion of climatic conditions and biomes on tropical land area
202 (Fig. 1a-b; Extended Data Fig. 1). The network is climatologically representative for 66% of the
203 pantropical land area with woody vegetation and matches pantropical distributions of
204 precipitation regimes reasonably well (Fig. 1b). The network overrepresents Northern
205 Hemisphere subtropical montane regions, where the presence of coniferous species facilitates
206 dendrochronology; while it underrepresents humid lowland tropical forests, in part because
207 weak climatic seasonality hampers chronology development[25]. We consider this over- and
208 under-representation by validation tests and weight-adjusted analyses.

209

210 **Four robust clusters of climate responses**

211 When SOM-clustering the chronologies according to their monthly climate responses, four
212 distinct groups with characteristic climate response modes emerge. Three of the four
213 climate response groups are globally distributed, taxonomically diverse, and climatologically
214 representative for 46-67% of global tropical woody vegetation (Fig. 1c). One of the groups
215 ('Strong positive P response') is restricted to North America, taxonomically poor, and has a
216 very limited representativeness (4%; Fig 1c).

217 Tree growth in three of the four groups responds positively to P increases and
218 negatively to T_{max} increases, supporting hypothesis 1, whereas these responses are reversed
219 in the fourth group ('Weak negative P response'; Fig. 2a). Despite differences in response
220 magnitude between the first three groups, the seasonality of the response is similar, with

the strongest climate responses occurring in the dry season (Fig. 2a). This larger importance of dry-season climate contrasts with hypothesis 2 and suggests dry-season water availability and demand as first-order drivers of interannual variability in tropical tree growth. The importance of this driver is further supported when ranking the groups from strongly positive P response to weakly negative P response. This ranking coincides with a gradient of low to high annual water availability (MAP and CWD; Fig. 2b) and strongly to weakly negative water balance (Extended Data Table 2), in accordance with hypothesis 3.

In the geographically restricted 'Strong positive P response' group, tree growth reacts strongly and positively to higher P and lower T_{max} throughout the dry season, with a response peak in the mid-dry season (Fig. 2a). At the semi-arid, high-elevation sites in this group, the mid-dry season occurs in winter, when P primarily falls as snow and becomes gradually available as moisture during spring when trees resume growth.

Trees in the 'Positive P response' and 'Weak positive P response' groups typically grow at lower elevation, at sites with low to medium water availability (Extended Data Table 2). In both groups, P response peaks in the late dry season, but the timing and shape of the peaks differ between groups. Finally, the 'Weak negative P response' group occurs at sites with relatively high water availability and is the only group with consistently negative P and positive T_{max} responses, that are somewhat stronger in the wet season compared to the dry season.

The two groups with the strongest positive P responses differ from each other not only in mean hydroclimatic conditions, but also in the amplitude of interannual P variation (Fig. 2c). Both annual and dry-season P variability are stronger for the 'Strong positive P response' group compared to the 'Positive P response' group, indicating that the strongest

climate responses can be found at dry sites with high P variability. In contrast, the two groups with the weakest climate responses show no significant differences in P variability, but differ in their P seasonality (Fig. 2d). Sites with a weakly positive P response have lower P seasonality and higher monthly dry-season P than sites with a weakly negative P response.

Climate response groups also differed in associations with El Niño Southern Oscillation (ENSO) cycle, a major driver of tropical forest productivity[8]. During El Niño years tree growth in the 'Strong positive P response' group is clearly stimulated, but associations are lacking or weak in the other groups (Extended Data Table 2).

The typical climate responses of these four groups are conserved in cross-validation tests in which a random portion (10%) or the overrepresented colder sites (MAT <10°C) were removed (Extended Data Fig. 2a-b). Validation tests in which poorly represented climates (MAP >2000 mm) and regions (Africa, Indonesia & Australia) were removed yielded high levels of correct assignments to climate response groups (Extended Data Fig. 2c-e). Region-specific cluster analyses (North America, High-mountain Asia, and South America) show consistent climate responses with the pantropical analysis (Extended Data Fig. 3; Extended Data Table 3). Thus, the climate response groups identified here are overall robust, unaffected by climatic over-/under-representation and also manifest themselves at the regional scale.

Seasonal climate responses vary with hydroclimate

To evaluate the climatic drivers of tropical tree growth at the seasonal level, we constructed multiple regression models for all individual chronologies. In 75% of these 347 regressions,

we found at least one significant effect of seasonal P or T_{max}. The regression coefficients reveal that effects of P and T_{max} on tree growth are equally large but mostly have opposite signs (P: positive; T_{max}: negative; Fig. 3a-b), in agreement with hypothesis 1.

Dry-season conditions were a stronger driver than wet-season conditions as indicated by a higher number of significant coefficients (262 dry-season vs. 176 wet-season coefficients, dry/wet ratio of coefficients = 1.5), larger absolute coefficient values (Fig. 3c), and higher relative importance values (Fig. 3d) for the dry season. Higher proportions of significant dry-season coefficients were found for all three positive P effects groups (dry/wet ratio ranging from 1.4-3.0). To examine the possible effect of rainfall timing during the late dry season, we ran regression models that included P and T_{max} during the last two months. While late dry season climate was often significant in these models, the absolute value of coefficients and their importance values were smaller than those of the full dry season (Extended Data Fig. 4). Together, these results contrast our expectation that tree growth is mostly driven by wet-season climate (hypothesis 2).

Hydroclimatic conditions likely modify these seasonal climate responses. We therefore performed weighted rank correlations between regression coefficients and climatic variables. These correlations show that the predominantly negative effect of dry-season T_{max} on tree growth is stronger at sites that are hotter, more arid, or experience a higher P variability (Fig. 3e-g, Extended Data Fig. 5), supporting hypothesis 3. In addition, we also find that positive dry-season P effects are stronger at drier sites (Fig. 3e). A notable exception to this general picture is the weaker positive dry-season P response at the warmest sites (Fig. 3g), which may be caused by stronger evapotranspiration demand, limiting the positive effects of a wetter dry season. The results of the unweighted correlation

289 analyses were similar to the weighted analyses for all tested climate variables except for
290 MAT (Extended Data Table 4). Thus, overall, dry-season climate responses are stronger
291 where water supply is low and evapotranspiration demand is high.

292

293 **A dominant role for dry-season climate variability**

294 Combined, our regression and cluster analyses show that tropical tree growth variability
295 responds primarily to dry-season climate variation and that this response is amplified in
296 regions that are drier, hotter, and experience stronger interannual climate variation. The
297 pantropical and multi-decadal scale of our study provides a context to short-term or regional
298 field studies that reported stronger drought-induced growth reduction at more arid
299 sites[20,26,27] (consistent with our tests of hypothesis 3) or absence of such responses[28,29]
300 (consistent with the 'Weak negative P response' group). The variability of climate responses
301 revealed by our study calls for caution in scaling up results of local or short-term studies[26,28].

302 Our finding of opposite and additive effects of P and T_{max} suggests a dominant role of
303 tree water balance (i.e., uptake from precipitation minus loss by transpiration) in driving
304 tropical tree growth. This is further supported by increased strength of P and T_{max} effects at
305 more arid sites. The importance of tree water balance can be understood from the basic
306 biology of xylem cell formation and enlargement[30] and their strong dependence on xylem
307 turgor pressure[31]. Xylem growth is promoted by high soil water availability, but diminished
308 by T_{max}-induced increase in vapour pressure deficit (VPD) and transpiration[26]. Alternative
309 mechanisms explaining the negative temperature effects on growth include T_{max}-induced
310 reduction in photosynthesis and increase in respiration[14], but their contribution is likely
311 small because T_{max} at our sites only rarely exceeds the thermal optimum for photosynthesis

(Supplementary Fig. 1) and because negative T_{max} effects occur across a wide range of MAT values (Fig. 3g).

We find that interannual variability in tropical tree growth is mostly explained by climatic variation during the dry season. This result contradicts our second hypothesis that at water-limited sites, wet-season climate drives annual tree growth and hence its interannual variability. How can the climate response of tree growth peak during the dry season, when the bulk of productivity of tropical trees growing in water-limited sites takes place during the wet season[20,26,32-35]? We hypothesize that dry-season climate is more important than wet-season climate because it is more variable (dry-season P variability = 30.9; wet-season P variability = 16.5, averaged across network) and because drier months within the dry season lead to direct reduction in tree available water, while the effect of such months during the wet season are likely buffered by soil water reserves[19]. We further hypothesize that climate conditions during the dry season constrain the magnitude of tree growth taking place during the following wet season, because climatologically benign dry seasons advance leaf flushing and xylem growth[20,26], thus extending the growing season. Detailed field studies are needed to quantify the physiological and phenological processes responsible for the observed strong dry-season effects and to improve their representation in process-based global vegetation models[36,37].

In addition to mean water availability as a first-order driver, climate responses of tropical tree growth are also modulated by the variability and seasonality in water availability. The effect of interannual variability in precipitation on the climate response of tree growth (Fig. 2c) is consistent with the larger contribution of arid regions to the interannual variation of the global carbon land sink[1,3]. Yet, the modifying role of P

seasonality on climate responses of tropical tree growth is poorly understood. The stronger P seasonality in the 'Weak negative P response' group (Fig. 2d) may occur if very low moisture availability during the dry season hampers photosynthesis and xylem growth, but also if root access to (deep) soil water during the dry season causes stem growth to be effectively insensitive to dry-season precipitation[38].

The positive T_{max} effects and negative P effects on tree growth in the 'Weak negative P response' group (Fig. 2a) are likely explained by two distinct mechanisms. At high-elevation sites (>3000 m a.s.l., 40% of the group), low growing season temperature may override water availability as the primary constraint of tree growth[39], while at low elevation sites (<1500 m a.s.l., 25%), negative P responses may reflect radiation limitation of photosynthesis[19,20]. Yet, the minimum MAP (2000 mm) at which radiation limitation is thought to occur[19,20], is not reached by 83% of the low-elevation sites in this group, suggesting that local soil and terrain conditions may alter this generic climatic threshold[19].

Aggravated drought responses under climate change

What shifts in interannual variability of tropical tree growth can be expected under anthropogenic climate change? Global Circulation Models predict an average 0.5-0.7°C warming per decade until 2100 for our sites (Extended Data Table 5), likely resulting in stronger water deficits for most of the sites. Drawing from the climatic variation in our network and the shifts in climate responses with MAT, CWD, and P variability, we expect continued climate change and increased P variability[40] to aggravate negative effects of hotter dry seasons and drier wet seasons on (regional) tree growth (Fig. 3e-g, Extended Data Fig. 5). This stronger sensitivity may elevate tree mortality[41,42], reduce tree longevity[43] and

increase the frequency of years that tropical vegetation flips from being a net carbon sink to a net source[8,15,16].

The climate responses of tropical tree growth revealed here, may aid the interpretation of interannual variability in the tropical land sink[3,6,10] as they provide field-based and region-specific insights into the climatic drivers of an important component of tropical vegetation productivity.

Acknowledgements

We acknowledge financial support for conducting the study by Agencia Nacional de Promoción Científica y Tecnológica, Argentina (PICT 2014-2797); Alberta Mennega Stichting; BBVA Foundation; Belspo BRAIN project: BR/143/A3/HERBAXYLAREDD; Confederação da Agricultura e Pecuária do Brasil - CNA; Coordenação de Aperfeiçoamento de Pessoal de Nível Superior - CAPES, Brazil (PDSE 15011/13-5, 88881.135931/2016-01, 88887.199858/2018-00, and Finance Code 001); Conselho Nacional de Desenvolvimento Científico e Tecnológico - CNPq, Brazil, (ENV 42, 1009/4785031-2, and 311874/2017-7); CONACYT-CB-2016-283134; CONICET; CUOMO FOUNDATION (IPCC scholarship); Deutsche Forschungsgemeinschaft - DFG (BR 1895/15-1, BR 1895/23-1, and BR 1895/29-1); DGD-RMCA PilotMAB; Dirección General de Asuntos del Personal Académico of the UNAM (Mexico); Elsa-Neumann-Scholarship of the Federal State of Berlin; EMBRAPA Brazilian Agricultural Research Corporation; Equatorian Dirección de Investigación UNL (21-DI-FARNR-2019); FAPESP São Paulo Research Foundation (2009/53951-7, 2012/50457-4, 2017/50085-3, 2018/01847-0, 2018/24514-7, 2019/08783-0, 2019/27110-7); FAPESP-NERC 18/50080-4; FAPITEC/SE and FUNTEC (01/2011); Fulbright Fellowship; German Academic Exchange Service (DAAD);

German Ministry of Education, Science, Research, and Technology (FRG 0339638); German Research Council (BR1895/24-1); ICRAF through the Forests, Trees, and Agroforestry research program of the CGIAR; Inter-American Institute for Global Change Research (IAI-SGP-CRA 2047); International Foundation for Science (D/5466-1); Lamont Climate Center; Miquelfonds; Minas Gerais Research Foundation FAPEMIG (APQ02541-14); National Geographic Global Exploration Fund (GEFNE80-13); USA's National Science Foundation NSF (IBN-9801287, 9553623, and a Postoctoral Fellowship); NSF P2C2 (AGS-1501321); NSF-FAPESP PIRE 2017/50085-3; NUFFIC-NICHE programme (HEART project); Peru 's CONCYTEC and World Bank (043-2019-FONDECYT-BM-INC.INV.); Peru's Fondo Nacional de Desarrollo Científico, Tecnológico y de Innovación Tecnológica (FONDECYT-BM-INC.INV 039-2019); Programa Bosques Andinos - HELVETAS Swiss Intercooperation; Programa Nacional de Becas y Crédito Educativo - PRONABEC; Schlumberger Foundation Faculty for the Future; Sigma Xi; Smithsonian Tropical Research Institute; Spanish Ministry of Foreign Affairs AECID (11-CAP2-1730); and UK NERC grant NE/K01353X/1. We thank logistical and field assistance by: Bangladesh Forest Department; Ethiopian Orthodox Tewahido Church and Congregants; Evandro Dalmaso (CEMAL logging firm); Instituto Boliviano de Investigación Forestal (IBIF; Bolivia); INPA parket Co.; Instituto Federal de Educação; Ciência e Tecnologia de Sergipe (IFS); Ministry of Minerals, Energy and Water Resources of Botswana; Reserva Natural da Vale (RNV); Sebastian Bernal; the Valere project of University of Campania "L. Vanvitelli"; the villagers of Nizanda in Oaxaca - Mexico. We acknowledge assistance and supervision by David Stahle, Dieter Eckstein, and Helene Muller-Landau.

Author contributions

P.A.Z, P.G. and V.T. initiated the tropical tree ring network; P.A.Z, F.B., P.G. and V.T. designed the study; all co-authors except F.B. contributed tree-ring data; F.B. and P.G. analysed the data, with important contributions from P.A.Z.; P.A.Z. and V.T. wrote the manuscript, with important contributions from F.B. and P.G.. All co-authors read and approved the manuscript.

Competing interests

The authors declare no competing interests.

Figure captions

Figure 1 | Distribution and climatic representativeness of tropical tree-ring network. a, Geographic distribution of tropical tree-ring chronologies (*n* = 347) on a tree cover map. **b,** Climatic representativeness of the network can be assessed based on distributions of chronologies (black) and tropical land area with woody vegetation (green). Density values are scaled from 0-1, with 1 indicating a condition that is most represented in the network (black) or occupies most land area (green). Climatic overrepresentation (underrepresentation) of network occurs when black lines are above (below) green lines. CWD: annual cumulative water deficit, MAP: mean annual precipitation, MAT: mean annual temperature, P seasonality: seasonality in precipitation, P variability: interannual variation in precipitation. **c,** Geographic distribution of four groups of tropical tree growth responses to climatic variation (*n* = 43, 69, 115, and 120 chronologies, respectively). Maps are coloured by water deficit (CWD) for pixels with woody vegetation falling within group-specific climate

envelops (MAT vs MAP) or are grey for woody vegetation pixels outside envelops. Groups are representative of 4, 48, 67, and 46% of woody vegetated tropical land area, respectively.

Figure 2 | Four climate response groups of tropical trees and their hydroclimatic differences. a, Relationships between ring-width index (RWI) and interannual variation in monthly T_{max} (red) or P (blue) of four climate response groups. Shown are Pearson *r* correlation coefficients (mean and 95% confidence intervals) for a 24-month period that covers the year of ring formation ('current') and that prior to ring formation ('previous'). Grey shading indicates wet-season timing. **b,** Distribution of mean water availability metrics that distinguish the first two from the last two groups. **c**, Distribution of climate variability metrics that distinguish the strongly positive from the positive P response group (P/DSP variability: interannual variability in annual/dry-season precipitation). **d,** Distribution of climate seasonality that distinguish the weakly positive from the negative P response group (DSP: dry season precipitation). Different letters denote significant differences between climate response groups (Wilcoxon rank sum test; $p<0.05$; Extended Data Table 2). Horizonal lines represent medians.

Figure 3 | Seasonal climate responses of tropical tree growth and their relation to hydroclimate. **a-b,** Distributions of significant regression coefficients for seasonal T_{max} (red) and P (blue) in multiple regression models of ring-width index (RWI). Letters denote differences between groups (Wilcoxon rank test, $p<0.05$, n = 438 coefficients; dry season: n = 262; wet season: n = 176). Horizonal lines represent medians. **c-d,** As panels a-b but for relative importance (models with >1 coefficient, n = 322 coefficients). **e-g,** Association of regression coefficients for dry-season P (blue, n = 130) and T_{max} (red, n = 132) with site

hydroclimate conditions. Symbol size is proportional to site hydroclimate representativeness (density values, Fig. 1b). Significant associations are indicated (weighted Spearman rank correlation; **: p <0.01; ***: p <0.001; Extended Data Table 3) and lines are shown for illustration only. All hydroclimatic variables are ordered from arid (left) to humid (right).

Figure captions

1 Ahlström, A. *et al.* The dominant role of semi-arid ecosystems in the trend and variability of the land CO2 sink. *Science* **348**, 895-899, doi:10.1126/science.aaa1668 (2015).

2 Friedlingstein, P. *et al.* Global Carbon Budget 2019. *Earth Syst. Sci. Data* **11**, 1783-1838, doi:10.5194/essd-11-1783-2019 (2019).

3 Poulter, B. *et al.* Contribution of semi-arid ecosystems to interannual variability of the global carbon cycle. *Nature* **509**, 600-603, doi:10.1038/nature13376 (2014).

4 Fan, L. *et al.* Satellite-observed pantropical carbon dynamics. *Nature Plants*, doi:10.1038/s41477-019-0478-9 (2019).

5 Humphrey, V. *et al.* Sensitivity of atmospheric CO2 growth rate to observed changes in terrestrial water storage. *Nature* **560**, 628-631, doi:10.1038/s41586-018-0424-4 (2018).

6 Jung, M. *et al.* Compensatory water effects link yearly global land CO 2 sink changes to temperature. *Nature* **541**, 516-520, doi:10.1038/nature20780 (2017).

7 Wang, J., Zeng, N. & Wang, M. Interannual variability of the atmospheric CO 2 growth rate: roles of precipitation and temperature. *Biogeosciences* **13**, 2339-2352 (2016).

8 Wigneron, J.-P. *et al.* Tropical forests did not recover from the strong 2015–2016 El Niño event. *Science Advances* **6**, eaay4603, doi:10.1126/sciadv.aay4603 (2020).

9 Keenan, T. F. & Williams, C. A. The Terrestrial Carbon Sink. *Annu. Rev. Environ. Resour.* **43**, 219-243, doi:10.1146/annurev-environ-102017-030204 (2018).

10 Niu, S. *et al.* Interannual variability of ecosystem carbon exchange: From observation to prediction. *Global Ecology and Biogeography* **26**, 1225-1237, doi:10.1111/geb.12633 (2017).

11 Fatichi, S., Pappas, C., Zscheischler, J. & Leuzinger, S. Modelling carbon sources and sinks in terrestrial vegetation. *New Phytologist* **221**, 652-668, doi:10.1111/nph.15451 (2019).

12 Zuidema, P. A., Poulter, B. & Frank, D. C. A Wood Biology Agenda to Support Global Vegetation Modelling. *Trends in Plant Science* **23**, 1006-1015, doi:10.1016/j.tplants.2018.08.003 (2018).

13 Moore, S. *et al.* Forest biomass, productivity and carbon cycling along a rainfall gradient in West Africa. *Glob. Chang. Biol.* **24**, e496-e510, doi:10.1111/gcb.13907 (2018).

14 Clark, D. A., Clark, D. B. & Oberbauer, S. F. Field-quantified responses of tropical rainforest aboveground productivity to increasing CO2 and climatic stress, 1997-2009. *Journal of Geophysical Research: Biogeosciences* **118**, 783-794 (2013).

15 Phillips, O. L. *et al.* Drought sensitivity of the Amazon rainforest. *Science* **323**, 1344-1347, doi:10.1126/science.1164033 (2009).

16 Hubau, W. *et al.* Asynchronous carbon sink saturation in African and Amazonian tropical forests. *Nature* **579**, 80-87, doi:10.1038/s41586-020-2035-0 (2020).

17 Pan, Y. *et al.* A large and persistent carbon sink in the world's forests. *Science* **333**, 988-993 (2011).

18 Anderegg, W. R. L. *et al.* Climate-driven risks to the climate mitigation potential of forests. *Science* **368**, eaaz7005, doi:10.1126/science.aaz7005 (2020).

19 Guan, K. *et al.* Photosynthetic seasonality of global tropical forests constrained by hydroclimate. *Nature Geoscience* **8**, 284-289, doi:10.1038/ngeo2382 (2015).

20 Wagner, F. H. *et al.* Climate seasonality limits leaf carbon assimilation and wood productivity in tropical forests. *Biogeosciences* **13**, 2537-2562, doi:10.5194/bg-13-2537-2016 (2016).

21 Zhang, X. *et al.* Dominant regions and drivers of the variability of the global land carbon sink across timescales. *Glob. Chang. Biol.* **24**, 3954-3968, doi:10.1111/gcb.14275 (2018).

22 Sullivan, M. J. P. *et al.* Long-term thermal sensitivity of Earth's tropical forests. *Science* **368**, 869-874, doi:10.1126/science.aaw7578 (2020).

23 Hewitson, B. & Crane, R. G. Self-organizing maps: applications to synoptic climatology. *Climate Research* **22**, 13-26 (2002).

24 Babst, F. *et al.* Twentieth century redistribution in climatic drivers of global tree growth. *Science Advances* **5**, eaat4313, doi:10.1126/sciadv.aat4313 (2019).

25 Groenendijk, P., Sass-Klaassen, U., Bongers, F. & Zuidema, P. A. Potential of tree-ring analysis in a wet tropical forest: A case study on 22 commercial tree species in Central Africa. *For. Ecol. Manage.* **323**, 65-78 (2014).

26 Rifai, S. W. *et al.* ENSO Drives interannual variation of forest woody growth across the tropics. *Philosophical Transactions of the Royal Society B: Biological Sciences* **373**, 20170410 (2018).

27 López, L., Rodríguez-Catón, M. & Villalba, R. Convergence in growth responses of tropical trees to climate driven by water stress. *Ecography* **42**, 1899-1912 (2019).

28 Doughty, C. E. *et al.* Drought impact on forest carbon dynamics and fluxes in Amazonia. *Nature* **519**, 78-82, doi:10.1038/nature14213 (2015).

29 Clark, D. A., Piper, S. C., Keeling, C. D. & Clark, D. B. Tropical rain forest tree growth and atmospheric carbon dynamics linked to interannual temperature variation during 1984–2000. *Proceedings of the National Academy of Sciences* **100**, 5852-5857, doi:10.1073/pnas.0935903100 (2003).

30 Rathgeber, C. B. K., Cuny, H. E. & Fonti, P. Biological Basis of Tree-Ring Formation: A Crash Course. *Frontiers in Plant Science* **7**, 734, doi:10.3389/fpls.2016.00734 (2016).

31 Peters, R. L. *et al.* Turgor–a limiting factor for radial growth in mature conifers along an elevational gradient. *New Phytologist*.

32 Trouet, V., Mukelabai, M., Verheyden, A. & Beeckman, H. Cambial growth season of brevi-deciduous Brachystegia spiciformis trees from South Central Africa restricted to less than four months. *PLoS One* **7**, e47364, doi:10.1371/journal.pone.0047364 (2012).

33 Mendivelso, H. A., Camarero, J. J., Gutiérrez, E. & Castaño-Naranjo, A. Climatic influences on leaf phenology, xylogenesis and radial stem changes at hourly to monthly scales in two tropical dry forests. *Agricultural and Forest Meteorology* **216**, 20-36, doi:10.1016/j.agrformet.2015.09.014 (2016).

34 Girardin, C. A. J. *et al.* Seasonal trends of Amazonian rainforest phenology, net primary productivity, and carbon allocation. *Global Biogeochemical Cycles* **30**, 700-715, doi:10.1002/2015GB005270 (2016).

35 Krepkowski, J., Bräuning, A., Gebrekirstos, A. & Strobl, S. Cambial growth dynamics and climatic control of different tree life forms in tropical mountain forest in Ethiopia. *Trees* **25**, 59-70, doi:10.1007/s00468-010-0460-7 (2011).

36 Restrepo-Coupe, N. *et al.* Do dynamic global vegetation models capture the seasonality of carbon fluxes in the Amazon basin? A data-model intercomparison. *Glob. Chang. Biol.* **23**, 191-208, doi:10.1111/gcb.13442 (2017).

37 Barichivich, J. *et al.* A triple tree-ring constraint for tree growth and physiology in a global land surface model. *Biogeosciences Discuss.* **2020**, 1-36, doi:10.5194/bg-2020-446 (2020).

38 Nepstad, D. C. *et al.* The role of deep roots in the hydrological and carbon cycles of Amazonian forests and pastures. *Nature* **372**, 666-669, doi:10.1038/372666a0 (1994).

39 Panthi, S., Fan, Z. X., van der Sleen, P. & Zuidema, P. A. Long-term physiological and growth responses of Himalayan fir to environmental change are mediated by mean climate. *Glob. Chang. Biol.* **26**, 1778-1794, doi:10.1111/gcb.14910 (2020).

40 Morales, M. S. *et al.* Six hundred years of South American tree rings reveal an increase in severe hydroclimatic events since mid-20th century. *Proceedings of the National Academy of Sciences*, 202002411, doi:10.1073/pnas.2002411117 (2020).

41 Brodribb, T. J., Powers, J., Cochard, H. & Choat, B. Hanging by a thread? Forests and drought. *Science* **368**, 261, doi:10.1126/science.aat7631 (2020).

42 McDowell, N. G. *et al.* Pervasive shifts in forest dynamics in a changing world. *Science* **368**, eaaz9463, doi:10.1126/science.aaz9463 (2020).

43 Locosselli, G. M. *et al.* Global tree-ring analysis reveals rapid decrease in tropical tree longevity with temperature. *Proceedings of the National Academy of Sciences*, 202003873, doi:10.1073/pnas.2003873117 (2020).

551

552

553

554

555

Methods

Tree-ring network. We established our tropical tree-ring network by compiling published ring-width chronologies from naturally regenerating tree populations in tropical and subtropical vegetation (30°N to 30°S; excluding mangroves and flooded forests). For this purpose, we compiled raw ring-width data from the International Tree-Ring Data Bank (ITRDB, https://www.ncdc.noaa.gov/data-access/paleoclimatology-data/datasets/tree-ring; 241 chronologies). To increase representation of wetter tropical regions[44,45], we complemented this data set with 174 chronologies derived from published tree-ring studies (mainly low-latitude sites; Extended Data Fig. 1).

Chronology selection. From the initial 415 chronologies, we selected those with a minimum length of 50 years, based on at least 5 trees, and ending after 1975. The 1975 cutoff date is a compromise between the low quality of early-20th century gridded climate data and the sharp recent decline in tree-ring data[46]. In addition, we selected chronologies with a mean inter-series correlation (Rbar) greater than 0.3 (see next Section) over the 50-year period. Low or non-significant Rbar-values may indicate poor dating quality, a lack of common environmental drivers of growth[47,48], or both, and are expected in wetter climates. By introducing an Rbar threshold, which removed 9% of chronologies, we sought a compromise between ensuring chronology quality and being overly selective towards highly climate-sensitive chronologies.

Our selection procedure removed 68 chronologies (6 ITRDB and 62 contributed). The resulting network includes 347 chronologies (235 from ITRDB, 112 from contributors) and is based on 7751 trees and 14,032 series from 99 species (56 genera, 24 families; metadata in

578 Supplementary Data 1). Species are represented by 1-49 chronologies (average = 3.4) and by
579 an average of 21.5 trees.

580 The selected chronologies were originally developed for various purposes, including climate
581 reconstructions, ecological studies, and timber yield evaluations. Dendroclimatic
582 reconstructions are usually conducted in marginal habitats in arid and high montane
583 regions[49], which may introduce a 'macro-site selection bias' in tree-ring networks. Such bias
584 can be strong, for instance in the arid Southwest of the United States[50], but were not found
585 to exist when ITRDB chronologies were compared to independent reference networks (Fig.
586 S7 in Ref 51; Fig. 3 in Ref 52). We accommodated possible 'macro-site selection bias' in our
587 network by calculating and accounting for the climatic representativeness of sites (see
588 'Network representativeness')[50].

589 **Chronology building and quality control.** To ascertain homogeneous data treatment across
590 trees and sites, we applied the same detrending method to all individual raw ring-width
591 series to develop tree-ring chronologies, rather than using the published chronologies. We
592 tested various detrending methods that account for ontogeny, remove low-frequency
593 variation, and retain the high-frequency (annual) variation we study here. We selected a
594 flexible spline detrending with a 50% frequency cut-off at 30 years to emphasize the
595 interannual variation in ring width. We developed mean chronologies of ring-width index
596 (RWI) from the detrended series using a bi-weight robust mean and the most recent 50
597 years of each chronology were selected for analysis. We ensured that dating of all tree-ring
598 series from the Southern Hemisphere followed the Schulman convention[53], such that the
599 calendar year assigned to the ring is that during which ring formation started. An exception
600 was made for the Southern Hemisphere chronologies in the Brazilian Caatinga biome, where

601 the growth season occurs between March and July[54] and thus coincides with the Northern
602 Hemisphere's growth season, making the Shulman shift redundant. Detrending and
603 chronology building was conducted in R (Ref 55) using the dplR package[56].

604 **Woody vegetation and elevation data.** To relate climate responses to tree cover, we
605 obtained MODIS-derived tree-cover percentages for all sites ('Percent_Tree_Cover',
606 MOD44B, version 6; https://lpdaac.usgs.gov/products/mod44bv006/). We also used this
607 data product to mask out areas with <10% tree cover of tropical land area.
608
609 **Climate data.** We used three types of gridded climate data. We used Worldclim version 2
610 (worldclim.org)[57] to obtain 30-year (1970-2000) mean annual and monthly climate
611 conditions at 1-km spatial resolution. This yielded data on mean monthly precipitation (P),
612 total dry-season precipitation (DSP, in mm), total wet-season precipitation (WSP, in mm),
613 mean annual precipitation (MAP, in mm), mean annual temperature (MAT, in °C), and
614 seasonality in precipitation (P seasonality, unitless; this is the coefficient of variation of
615 monthly P[57]). In addition, we calculated the monthly climatic water balance (CWB) as the
616 difference between monthly precipitation and potential evapotranspiration (P-PET). PET was
617 estimated from monthly Worldclim climate parameters using the Penman-Monteith
618 equation implemented in the *SPEI* package in R (Ref 58). From these data we derived per
619 site: annual climatic water deficit (CWD, in mm; always negative) as the sum of all negative
620 monthly CWBs, annual CWB (in mm) as the sum of all monthly CWBs, and maximum monthly
621 water deficit (MMWD, in mm) as the lowest (i.e., most negative) value of monthly CWBs.
622 This set of variables was used to characterize climatic site conditions for all chronologies.
623 We further used Worldclim to obtain CMIP6 downscaled future climate projections for
624 periods 2041-2060 and 2061-2080 (compared to 1970-2000) for all sites. We used two

625 Shared Socio-economic Pathways (SSPs): 370 and 585, and 9 Global Circulation Models
626 (GCMs) of which we calculated an ensemble (arithmetic) mean across sites and GCMs.
627 Third, we used CRU TS4.02 (Ref 59) climate data to conduct climate-growth analyses based
628 on monthly time series at a coarser spatial resolution (0.5°) for the most recent 50 years of
629 each chronology in our network. Such broader resolution gridded data do not optimally
630 capture elevational climate gradients, but they provide the homogeneity and long time
631 series needed to establish climate-growth relations in our cluster and regression analyses. All
632 climate-growth analyses were conducted for T_{max} (daily maximum temperature, averaged
633 per month or season) and P (precipitation, sum per month or season). We chose to use T_{max}
634 as it is related to atmospheric drought (Vapour Pressure Deficit, VPD) and thus to the tree
635 water balance, which we hypothesized to be an important driver of tropical tree growth.
636 CRU data were also used to obtain a metric of interannual variation in P (P variability) for all
637 sites and for all tropical land with woody vegetation. P variability was calculated as the
638 coefficient of variation of the P time series over the 50 years covered by the tree-ring
639 chronologies.

640 **Season definitions.** The multiple regression models (see below) were constructed for
641 seasonal (wet and dry season) P and T_{max}. We tested various season definitions based on P
642 and CWB: seasons based on a monthly P cut-off of 50 and 100 mm[45] and based on CWB
643 calculated using the Thornthwaite and the Penman-Monteith equations. Seasonal
644 boundaries were very similar for 100 mm P, and CWB (Penman-Monteith) definitions and we
645 thus selected the 100 mm cut-off definition for its simplicity and because variables such as
646 wind speed required for CWB are associated with large uncertainties in gridded data. The
647 dry season was thus defined as all months with less than 100 mm precipitation preceding
648 the wet season of the year of ring formation.

649

650 **Frequency of hot months.** To estimate to which extent T_{max} may limit tree growth through
651 decreased photosynthesis, we calculated per site the percentage of months during which
652 T_{max} exceeded 30°C, when leaves in sun-exposed crowns can reach temperatures >32°C and
653 reduce photosynthesis[60,61]. If a large proportion of sites frequently experiences such high
654 T_{max} values, this suggests an important role of temperature-driven photosynthetic limitation
655 in tropical tree growth. If that proportion is small, it suggests that negative effects of T_{max} on
656 tropical tree growth are mainly resulting from increased transpiration.

657

658 **Network representativeness.** We evaluated the climatic representativeness of our network
659 in two ways. First, we used Worldclim average climate data for all sites to define the climate
660 space of our network and the four climate response groups (see below under 'Cluster
661 analysis'), using a convex hull that encompasses 99% of the network's MAP and MAT range
662 (i.e., to minimize edge effects). Grid cells with MAP-MAT combinations outside this contour
663 shape are not represented by our network and masked from CWD maps (Fig. 1c). Climatic
664 representativeness was estimated by calculating the percentage of pixels of tropical land
665 area with >10% woody vegetation (49,870,418 km^2) within the convex hull.
666 Second, we quantified the representativeness of our network for tropical vegetation by
667 comparing the probability density distributions of geographic and climatic variables (CWD,
668 MAP, P seasonality, P variability, MAT) across our sites with those of all tropical land area
669 that supports woody vegetation (>10% tree cover). We scaled both sets of distributions (i.e.,
670 sites and land area) by dividing them by their maximum values. Thus, a scaled value of 0
671 implies that the corresponding climatic condition is not represented by sites or tropical land
672 area; a value of 1 implies that the climatic condition has the highest representation of sites

673 or land area. When the scaled distributions of the network (black lines in Fig. 1b) and tropical
674 land area (green lines) are similar, overall representativeness is good (e.g., MAT, P variability;
675 Fig. 1b); if they are dissimilar, overall representativeness is limited (e.g., MAT). For each
676 climatic variable, a higher value of the network compared to the tropical land area indicates
677 overrepresentation in the network, while the reverse indicates underrepresentation. We use
678 the scaled distributions of land area for weighted correlations in our analysis of shifts in
679 climate responses along climatic gradients (see below under 'Climate responses vs. climatic
680 conditions'). In two-dimensional space (Fig. 1b), distributions were calculated using bivariate
681 kernel density estimation (GenKern package[62]).
682

683 **Cluster analysis.** Seasonal climate-growth analyses can miss subtle, idiosyncratic responses
684 of tree species to climatic conditions during specific months or with a lag period. To
685 accommodate such responses, we conducted monthly climate-growth analyses (simple
686 Pearson correlations) for a 24-month period (full year of ring formation, plus full previous
687 year) and used these as a basis for clustering. For Northern Hemisphere sites, the 24-month
688 period starts in January of the year prior to ring formation and ends in December of the year
689 of ring formation. For Southern Hemisphere sites, this period is lagged by 6 months (running
690 from July-1 to June). We identified distinct groups of sites with a coherent climate response
691 using self-organizing maps (SOMs[63]). SOMs are an artificial neural network-based method of
692 dimension reduction that assigns observations (chronologies) to a set of clusters (or
693 "nodes") based on Euclidian distance. In an iterative process, the optimal node assignment is
694 determined in an unsupervised manner to best represent the dataset's variance. Nodes are
695 then arranged in a grid of definable size and shape: closer nodes in this grid are more similar,
696 distant nodes are dissimilar. This feature greatly facilitates the visualization and

interpretation of nodes, as has previously been shown in regional and continental-scale tree-ring studies[64,65].

We calculated SOMs based on the monthly climate correlations. The algorithm was presented with 24 T_{max} correlations and 24 P correlations per site, but no other information (e.g., site location or climate). We tested square SOM-grids of increasing size (2x2, 3x3, etc.) to visualize increasingly nuanced differences in climate response between the nodes. Then, we calculated bootstrapped means (1000 replicates) and 95% confidence intervals of the climate correlations from all sites (Fig. 2a) or that of geographic sub-regions (Extended Data Fig. 4) that were assigned to a given node. We present the results based on the 2x2 SOM-grid (i.e., four climate response groups). Further subdivision did not result in additional modes of climate response, but merely in minimally differing variants of the four main groups. While SOM clustering uses all subtleties of site-specific responses of RWI to monthly climate conditions, the resulting climate responses are an average across all sites within a cluster and may therefore differ from site-specific correlation patterns. Despite this possible discrepancy, SOM clustering optimizes the representation of idiosyncratic and subtle climate responses of tree growth.

One challenge associated with SOMs is that their initiation is random, which leads to minor differences in site assignments. To overcome this challenge, we stabilized the grouping iteratively in 10,000 consecutive SOM runs. In each run, the codebook vectors (representing the mean climate correlations within a node) were reassigned to an existing node with the most similar codebook vector based on all prior runs. This codebook vector was then updated with the new vector. For the final site assignment, we considered only the last 1000 runs, when the codebook vectors did not change much anymore. The percentage of those runs when a site was assigned to a given node (e.g., site X was assigned to Node1 in 900 out

of 1000 runs = 90%) was used as a quality measure for the clustering. Percentage assignments were high: 93 ±10% (mean ± 1 SD) across the entire network and ranging from 85-97% (means) per cluster. These analyses were performed using the *kohonen*[66] and *boot*[67] packages in R.

To compare climate and geographic characteristics of the four climate response groups, we performed non-parametric analyses of variance (Kruskal-Wallis rank sum test) followed by a Wilcoxon rank sum post-hoc test.

Validation tests of cluster analysis results. To evaluate the robustness of our cluster results regarding the over- and under-representation of climatic conditions and regions, we performed four sets of validation tests. In these 'leave-several-out-cross-validation' tests we removed a number of chronologies from the network: (1) a random subset to test overall robustness (10%, repeated 10 times); (2) all 'cold' sites (<10°C MAT) to test whether clustering is strongly driven by high-elevation sites that are overrepresented in our network; (3) all 'wet' sites (>2000 mm MAP), and (4) all sites in underrepresented regions (Africa, Indonesia & Australia), both with the goal to verify whether low representation of climates or regions affects the assignment of chronologies to climate response groups. After removing the sites, we reconducted the cluster analyses (as described above in 'Cluster analysis') for the remaining chronologies. Each of the removed sites was then 'assigned' to one of the four clusters by calculating monthly climate growth correlations with all four clusters and assigning it to the cluster with most similar climate correlation patterns (i.e., smallest average difference in monthly correlations). We then calculated the percentage of correct assignments (i.e., to the same cluster as in the original clustering approach) and compared monthly climate correlation patterns (Extended Data Fig. 2) with those of the

main analysis (Fig. 2a). Clustering results were considered robust if correlation patterns remain similar and the percentage of correct assignments is high.

Evaluating sensitivity of climate responses to quality of gridded climate data. To evaluate possible biases introduced by spatially varying quality of gridded climate data, we performed two analyses using distance of sites to the nearest meteorological station (from climexp.knmi.nl) as a proxy for the quality of gridded data. For the majority of sites, proximal meteorological stations exist: distances between sites and stations ranged from 0-243 km (median: 63 km) and were > 100 km for 93 sites (27%). Analysis 1: we evaluated associations between the seasonal climate response and the distance to nearest station. Because climate responses are driven by mean climate, we performed this analysis within two-way climate bins of MAP (300 mm wide) and MAT (3°C wide). Within each climate bin that contained at least 10 sites, we associated the climate response (i.e., the *p*-value of the Pearson correlation of RWI with P or T_{max} during dry or wet season) with distance to nearest meteorological station, using Spearman rank correlation. Positive Spearman correlations indicate that correlation strength is higher when meteorological station density is higher (Extended Data Table 1a). Analysis 2: to verify the extent to which climate responses in our four clusters are modulated by the density of meteorological stations, we used t-tests to find differences in correlation coefficients of RWI and monthly climate (P and T_{max}) between sites located <100 km and >100 km from meteorological stations. We conducted tests for the two climate response groups with a sufficiently large number (n >10) of sites at >100 km from meteorological stations and for the 24-month period used in our clustering analysis (Extended Data Table 1b).

Multiple regression analysis. For each chronology we ran a multiple regression model to evaluate additive effects on RWI of interannual variability in seasonal T_{max} and P, which typically co-vary. This approach allows for controlling for one variable while testing the effect of another and yields additive effects in case multiple variables are included. To prevent model overfitting, we limited the number of explanatory variables (summed P and average T_{max}) and conducted seasonal (rather than monthly) analyses. The maximum number of climate variables in the models is thus 4, for a fixed chronology length of 50 years. We used the leaps algorithm for model selection, an all-subset model comparison[68] that is more robust than stepwise methods. We scaled climate variables: their effects on tree growth are therefore directly comparable and unaffected by season length. We checked for collinearity between P and Tmax and found significant, mostly negative, associations in 73% (wet) and 59% (dry) of cases. We therefore checked Variance Inflation Factors (VIFs) in all models and found these to be lower than 2.2. To compare the relative strength of P and T_{max} effects on tree growth, we calculated relative importance values of significant climate variables. These are reported only for models with >1 significant coefficient.

To examine whether dry-season effects were mostly driven by P over the entire dry season or in the transitional months from dry to wet season (the 'Late dry season'), we also ran all regression models with two additional climate variables: summed P and average T_{max} over the two last months of the dry season, and then compared number of significant coefficients, absolute coefficient values, and relative importance values of full vs. late dry season (Extended Data Fig. 4). Analyses were conducted in R using packages *leaps*[69], *bestglm*[70] and *relaimpo*[71].

Climate responses vs. climatic conditions. To evaluate whether seasonal climate responses of tree growth are associated with site hydroclimate, we correlated significant regression coefficients with site climatic conditions: CWD, MAP, MAT, P variability, and P seasonality. We performed ordinary as well as weighted Spearman rank correlations, to account for climate representativeness of sites. We weighted data points by the relative density of tropical land area with woody vegetation for each climate variable (i.e., the green lines in Fig. 1b; see section 'Analyses of network representativeness'). Thus, low-MAT sites (overrepresented in network) received a lower weight than high-MAT sites. Analyses were conducted in R using package *expss*[72].

Data availability

The 50-year mean RWI time series of all 347 chronologies used in this study will be made available through Data Dryad (DOI: to be included upon publication). All relevant meta-data of these chronologies are included in Supplementary Data File S1. Raw tree-ring width data of 98 out of the 112 contributed chronologies used in the analyses will be uploaded to the International Tree-Ring Data Bank (ITRDB, https://www.ncdc.noaa.gov/data-access/paleoclimatology-data/datasets/tree-ring).

Code availability

R-code used for chronology construction and statistical analyses will be made available upon request.

References

44 Zhao, S. *et al.* The International Tree-Ring Data Bank (ITRDB) revisited: Data availability and global ecological representativity. *Journal of Biogeography* **46**, 355-368, doi:10.1111/jbi.13488 (2019).

45 Brienen, R. J., Schöngart, J. & Zuidema, P. A. in *Tropical Tree Physiology* 439-461 (Springer International Publishing, 2016).

46 Babst, F., Poulter, B., Bodesheim, P., Mahecha, M. D. & Frank, D. C. Improved tree-ring archives will support earth-system science. *Nature Ecology & Evolution* **1**, 0008, doi:10.1038/s41559-016-0008 (2017).

47 Fichtler, E., Clark, D. A. & Worbes, M. Age and Long-term Growth of Trees in an Old-growth Tropical Rain Forest, Based on Analyses of Tree Rings and 14C. *Biotropica* **35**, 306-317 (2003).

48 Groenendijk, P., Sass-Klaassen, U., Bongers, F. & Zuidema, P. A. Potential of tree-ring analysis in a wet tropical forest: A case study on 22 commercial tree species in Central Africa. *For. Ecol. Manage.* **323**, 65-78 (2014).

49 Fritts, H. *Tree rings and climate*. (Elsevier, 2012).

50 Klesse, S. *et al.* Sampling bias overestimates climate change impacts on forest growth in the southwestern United States. *Nat. Commun.* **9**, 5336, doi:10.1038/s41467-018-07800-y (2018).

51 Babst, F. *et al.* Twentieth century redistribution in climatic drivers of global tree growth. *Science Advances* **5**, eaat4313, doi:10.1126/sciadv.aat4313 (2019).

52 Klesse, S. *et al.* A Combined Tree Ring and Vegetation Model Assessment of European Forest Growth Sensitivity to Interannual Climate Variability. *Global Biogeochemical Cycles* **32**, 1226-1240, doi:10.1029/2017GB005856 (2018).

53 Schulman, E. *Dendroclimatic changes in semiarid America*. (University of Arizona Press, 1956).

54 Aragão, J. R. V., Groenendijk, P. & Lisi, C. S. Dendrochronological potential of four neotropical dry-forest tree species: Climate-growth correlations in northeast Brazil. *Dendrochronologia* **53**, 5-16, doi:10.1016/j.dendro.2018.10.011 (2019).

55 R Core Team. R: A language and environment for statistical computing. (R Foundation for Statistical Computing, Vienna, Austria., 2019).

56 Bunn, A. G. A dendrochronology program library in R (dplR). *Dendrochronologia* **26**, 115-124, doi:https://doi.org/10.1016/j.dendro.2008.01.002 (2008).

57 Fick, S. E. & Hijmans, R. J. WorldClim 2: new 1-km spatial resolution climate surfaces for global land areas. *International Journal of Climatology* **37**, 4302-4315, doi:10.1002/joc.5086 (2017).

58 Vicente-Serrano, S. M., Beguería, S. & López-Moreno, J. I. A multiscalar drought index sensitive to global warming: the Standardized Precipitation Evapotranspiration Index. *Journal of Climate* **23**, 1696-1718, doi:10.1175/2009jcli2909.1 (2010).

59 Harris, I., Jones, P. D., Osborn, T. J. & Lister, D. H. Updated high-resolution grids of monthly climatic observations – the CRU TS3.10 Dataset. *International Journal of Climatology* **34**, 623-642, doi:10.1002/joc.3711 (2014).

60 Pau, S., Detto, M., Kim, Y. & Still, C. J. Tropical forest temperature thresholds for gross primary productivity. *Ecosphere* **9**, e02311, doi:10.1002/ecs2.2311 (2018).

61 Mau, A., Reed, S., Wood, T. & Cavaleri, M. Temperate and tropical forest canopies are already functioning beyond their thermal thresholds for photosynthesis. *Forests* **9**, 47 (2018).

62 Lucy, D., Aykroyd, R. G. & Pollard, A. M. Nonparametric calibration for age estimation. *Journal of the Royal Statistical Society: Series C (Applied Statistics)* **51**, 183-196, doi:10.1111/1467-9876.00262 (2002).

63 Hewitson, B. & Crane, R. G. Self-organizing maps: applications to synoptic climatology. *Climate Research* **22**, 13-26 (2002).

64 Babst, F. *et al.* Site- and species-specific responses of forest growth to climate across the European continent. *Global Ecology and Biogeography* **22**, 706-717, doi:10.1111/geb.12023 (2013).

65 Martin-Benito, D. & Pederson, N. Convergence in drought stress, but a divergence of climatic drivers across a latitudinal gradient in a temperate broadleaf forest. *Journal of Biogeography* **42**, 925-937, doi:10.1111/jbi.12462 (2015).

66 Wehrens, R. & Buydens, L. M. Self-and super-organizing maps in R: the Kohonen package.

67 Canty, A. & Ripley, B. D. boot: Bootstrap R (S-Plus) Functions. R package version 1.3-26. (2021).

68 Furnival, G. M. & Wilson, R. W. Regressions by Leaps and Bounds. *Technometrics* **16**, 499-511, doi:10.2307/1267601 (1974).

69 Lumley, T. leaps: Regression Subset Selection. R package v. 3.1 (2019).

70 McLeod, A. I., Xu, C. & Lai, Y. bestglm: Best Subset GLM and Regression Utilities. R package 0.37.3 (2020).

71 Groemping, U. Relative Importance for Linear Regression in R: The Package relaimpo. *Journal of Statistical Software* **17**, 27, doi:10.18637/jss.v017.i01 (2006).

72 Demin, G. & Jeworutzki, S. expss: Tables, Labels and Some Useful Functions from Spreadsheets and 'SPSS' Statistics. R package 0.10.7 v. 0.10.7 (2020).

73 Whittaker, R. H. *Primary productivity of the biosphere.*, Vol. 14 339 (Springer-Verlag, , 1975).

74 Beck, H. E. *et al.* Present and future Köppen-Geiger climate classification maps at 1-km resolution. *Sci Data* **5**, 180214-180214, doi:10.1038/sdata.2018.214 (2018).

880

881

882

Extended Data Table 1 | Climate responses are robust to among-site variation in quality of gridded climate data. **a,** Results of Spearman rank correlations between *p*-values of seasonal climate responses (Pearson correlations of RWI vs. seasonal P and T_{max}) and distance to the nearest meteorological station (a quality proxy for gridded climate data). Rank correlations were conducted for MAP-MAT climate bins (bin size of 300mm MAP by 3°C MAT) that contained at least 10 sites. Only 15% of the correlations were significantly positive, suggesting a minor effect of data quality on the climate responses. **b,** Results of t-tests that compare monthly climate responses (Pearson correlation coefficients of RWI vs. monthly P and T_{max}) for sites close to (<100 km) or further away from (>100 km) a meteorological station. Tests were conducted for the 24-months period used in SOM-clustering analysis, and for two climate response groups with >10 sites at >100 km from meteorological stations. Significantly stronger climate response for sites closer to meteorological stations were found in just 8% of the cases, and the reverse was found for a similar proportion (7%). Thus, climate growth responses were consistent for sites located close to or far away from meteorological stations.

a. Result of Spearman's rank correlation:	**Dry-season:**		**Wet-season:**	
	P	**T_{max}**	**P**	**T_{max}**
Non-significant ($p \geq 0.05$)	8	10	8	11
Significantly negative ($p < 0.05$)	0	0	0	0
Significantly positive ($p < 0.05$)	4	2	1	0
Total number of tests (grand total = 46)	12	12	11	11
b. Result of t-test:	**'Weak positive P response' group**		**'Weak negative P response' group**	
	P	**T_{max}**	**P**	**T_{max}**
Non-significant ($p \geq 0.05$)	19	20	20	21

Stronger correlation for sites closer to meteorological station (p<0.05)	3	2	3	0
Stronger correlation for sites further away from meteorological station (p<0.05)	2	2	1	3
Total number of tests (grand total = 96)	24	24	24	24

898

899

Extended Data Table 2 | Characteristics of four climate response groups. Shown are counts (for variables starting with '#') and medians (all other variables) per climate response group. Different letters denote climate response groups with significantly different median values in a post-hoc test (Wilcoxon rank sum test; $p<0.05$; NS=not significant). Representativeness of geographic and climatic variables is shown as the mean of the scaled density of all sites in a climate response group for the climatic variable of interest. Rbar: mean inter-series correlation; MAT: mean annual temperature; MAP: mean annual precipitation; CWD: annual climatic water deficit; CWB: cumulative water balance; MMWD: maximum monthly water deficit; P seasonality: seasonality of monthly precipitation; P variability: inter annual variation in annual precipitation; DSP variability: inter annual variation in dry-season precipitation; P seasonality: precipitation seasonality; DSP: dry-season precipitation; WSP: wet-season precipitation; ENSO: El Niño Southern Oscillation.

		Climate response group			
		Strong positive P response	**Positive P response**	**Weak positive P response**	**Weak negative P response**
Basic information	#Chronologies	43	69	115	120
	#Countries	3	11	26	30
	% Woody vegetation area represented	3.5	47.7	67.2	46.3
	Standard deviation	0.23 [a]	0.21 [a]	0.21 [a]	0.18 [b]
	1-yr autocorrelation	-0.01 [d]	0.13 [c]	0.18 [b]	0.28 [a]
	Rbar	0.67 [a]	0.54 [b]	0.50 [c]	0.49 [c]
Geography	Latitude (° N or S)	25.4 [a]	20.1 [ab]	14.6 [b]	26.8 [a]
	Elevation (m a.s.l.)	2314 [a]	1300 [b]	1238 [b]	2685 [a]

Mean climate	MAT (°C)	11.8 ^{c}	20.1 ^{a}	19.3 ^{a}	16.1 ^{b}
	MAP (mm)	803 ^{b}	999 ^{a}	1125 ^{a}	1094 ^{a}
	CWD (mm)	-757 ^{c}	-524 ^{b}	-422 ^{a}	-381 ^{a}
	CWB (mm)	-728 ^{c}	-241 ^{b}	-244 ^{b}	-74 ^{a}
	MMWD (mm)	-127 ^{d}	-114 ^{c}	-90 ^{b}	-75 ^{a}
	# Wet months	3 ^{a}	4 ^{b}	5 ^{b}	4 ^{b}
Climate variability	P variability (-)	20.9 ^{a}	16.2 ^{b}	14.6 ^{b}	13.2 ^{c}
	DSP variability (-)	40.7 ^{a}	31.7 ^{b}	27.4 ^{c}	30.5 ^{c}
Climate seasonality	P seasonality (-)	90.0 ^{ab}	83.0 ^{bc}	82.9 ^{c}	89.5 ^{a}
	Precipitation Concentration Index (PCI)	14.7 ^{ab}	13.7 ^{bc}	13.7 ^{c}	14.8 ^{a}
	DSP (mm/month)	38.2 ^{ab}	34.9 ^{ab}	45.9 ^{a}	33.7 ^{b}
	DSP (mm/season)	347 ^{a}	263 ^{c}	323 ^{b}	254 ^{c}
	WSP (mm/month)	168 ^{NS}	163 ^{NS}	159 ^{NS}	175 ^{NS}
	WSP (mm/season)	515 ^{b}	744 ^{a}	786 ^{a}	815 ^{a}
ENSO responses	Pearson correlation with MEI (Multi-variate ENSO index) in current year	0.37 ^{a}	-0.12 ^{c}	-0.002 ^{c}	0.08 ^{b}
Species composition	#Species	8	22	61	50
	#Genera	4	9	37	28
	#Plant families	2	5	16	14
	#Angiosperm species	1	5	34	26
	#Angiosperm chronologies	1	22	55	40
Representa-tiveness	Latitude	0.62	0.67	0.69	0.66
	Elevation	0.06	0.34	0.31	0.16
	MAT	0.06	0.36	0.30	0.19
	MAP	0.91	0.87	0.89	0.87

	CWD	0.24	0.39	0.46	0.50
	P variability	0.41	0.66	0.71	0.77
	P seasonality	0.80	0.81	0.82	0.78

912

Extended Data Table 3 | Regional differences of climate response groups. Shown are counts (for variables starting with '#') and medians (all other variables) per climate response group and for each of three well-represented regions. Different letters denote groups with significantly different median values in a post-hoc test (Wilcoxon rank sum test; $p<0.05$; NS=not significant). Only groups represented by >10 sites were tested. MAT: mean annual temperature; MAP: mean annual precipitation; CWD: annual climatic water deficit; P seasonality: seasonality of monthly precipitation; P variability: inter annual variation in annual precipitation; DSP variability: inter annual variation in dry-season precipitation; P seasonality: precipitation seasonality; DSP: dry-season precipitation; WSP: wet-season precipitation.

North America		**Climate response group**			
		Strong positive P response	**Strong positive P response**	**Strong positive P response**	**Strong positive P response**
Basic info	#Chronologies	42	46	16	15
Geography	Elevation (m a.s.l.)	2332 ^{a}	1685 ^{b}	47 ^{c}	2500 ^{ab}
Mean climate	MAT (°C)	11.7 ^{c}	19.3 ^{b}	21.9 ^{a}	12.1 ^{c}
	MAP (mm)	803 ^{b}	856 ^{ab}	1255 ^{a}	966 ^{ab}
	CWD (mm)	-764 ^{b}	-646 ^{a}	-503 ^{b}	-549 ^{ab}
Climate variability	P variability (-)	20.9 ^{a}	17.7 ^{b}	15.3 ^{b}	18.3 ^{ab}
	DSP variability (-)	40.6 ^{a}	30.4 ^{b}	30.6 ^{b}	39.2 ^{a}
Climate seasonality	P seasonality (-)	90.1 ^{ab}	83.0 ^{ab}	61.3 ^{b}	95.7 ^{a}
	DSP (mm/month)	37.9 ^{NS}	35.8 ^{NS}	47.4 ^{NS}	30.9 ^{NS}
	WSP (mm/month)	168 ^{NS}	150 ^{NS}	169 ^{NS}	178 ^{NS}

High-mountain Asia

Basic info	#Chronologies	3	34	58
Geography	Elevation (m a.s.l.)		3100 [b]	3284 [a]
Mean climate	MAT (°C)		9.0 [NS]	11.0 [NS]
	MAP (mm)		841 [NS]	1094 [NS]
	CWD (mm)		-273 [NS]	-310 [NS]
Climate variability	P variability (-)		12.5 [NS]	12.6 [NS]
	DSP variability (-)		20.2 [NS]	26.7 [NS]
Climate seasonality	P seasonality (-)		84.2 [b]	94.2 [a]
	DSP (mm/month)		32.4 [a]	34.4 [b]
	WSP (mm/month)		170 [b]	196 [a]

South America

Basic info	#Chronologies		38	27
Geography	Elevation (m a.s.l.)		590 [NS]	1600 [NS]
Mean climate	MAT (°C)		21.8 [NS]	18.5 [NS]
	MAP (mm)		1140 [NS]	899 [NS]
	CWD (mm)		-491 [NS]	-178 [NS]
Climate variability	P variability (-)		17.0 [NS]	16.8 [NS]
	DSP variability (-)		24.0 [b]	28.5 [a]
Climate seasonality	P seasonality (-)		62.1 [NS]	83.8 [NS]
	DSP (mm/month)		48.2 [NS]	38.0 [NS]
	WSP (mm/month)		154.9 [NS]	151.3 [NS]

923

Extended Data Table 4 | Correlations of seasonal regression coefficients and site climate conditions. Results of unweighted (UW) and weighted (W) Spearman rank correlations between site climate variables (CWD, MAP, MAT, P variability, and P seasonality) and significant regression coefficients for P and T_{max} during dry (**a**) or wet (**b**) season. The weighted correlation analysis accounts for the under- and over-representation of climatic conditions in our network by weighing data points by the relative density of tropical woody vegetation for the value of the climate variable under consideration (green lines in Extended Data Fig. 2). A total of 438 significant regression coefficients were obtained from 260 multiple regression models that contained at least one significant effect (out of the 347 models conducted for all chronologies). Significance levels: *: 0.01<*p*<0.05; **: 0.001<*p*<0.01; ***: *p* <0.001. Sample sizes dry season: P, n=130; T_{max}, n=132; wet season: P, n=92; T_{max}, n= 84.

a. Dry season

		CWD		MAP		MAT		P variability		P seasonality	
		UW	W	UW	W	UW	W	UW	W	UW	W
P	T_{max}	**-0.259**	**-0.232**	-0.088	-0.002	0.002	**-0.367**	**0.232**	**0.232**	0.070	0.053
	P	**	**	NS	NS	NS	***	**	*	NS	NS
T_{max}	T_{max}	**0.425**	**0.390**	**0.317**	**0.307**	0.050	**-0.312**	**-0.341**	**-0.336**	0.015	-0.005
	P	***	***	***	***	NS	***	***	***	NS	NS

b. Wet season

		CWD		MAP		MAT		P variability		P seasonality	
		UW	W	UW	W	UW	W	UW	W	UW	W
P	T_{max}	-0.158	-0.077	-0.049	-0.019	**0.362**	0.181	**0.467**	**0.332**	**-0.273**	**-0.328**
	P	NS	NS	NS	NS	***	NS	***	**	**	**
T_{max}	T_{max}	0.027	0.066	0.046	0.102	-0.126	0.110	0.104	0.039	-0.010	-0.047
	P	NS	NS	NS	NS	NS	NS	NS	NS	NS	NS

Extended Data Table 5 | Predicted warming at network sites. Predicted maximum (T_{max}), minimum (T_{min}), and mean (T_{mean} =T_{max} - T_{min}) warming, averaged across all 347 sites until 2100, and relative to 1970-2000 values. For each site, predictions of 9 GCMs were averaged, and then site-specific values were averaged, and their SD calculated. Predictions are shown for two Shared Socio-economic Pathways (SSPs).

Predicted increase in:	SSP	2021-2040	2041-2060	2061-2080	2081-2100
T_{max} (°C)	370	1.32±1.24	2.21±1.27	3.21±1.31	4.35±1.37
	585	1.49±1.25	2.58±1.26	3.95±1.32	5.59±1.41
T_{min} (°C)	370	1.25±1.2	2.11±1.23	3.08±1.26	4.18±1.33
	585	1.37±1.21	2.44±1.23	3.77±1.3	5.36±1.42
T_{mean}(°C)	370	1.29±1.14	2.16±1.17	3.15±1.2	4.27±1.26
	585	1.43±1.14	2.51±1.16	3.86±1.22	5.47±1.32

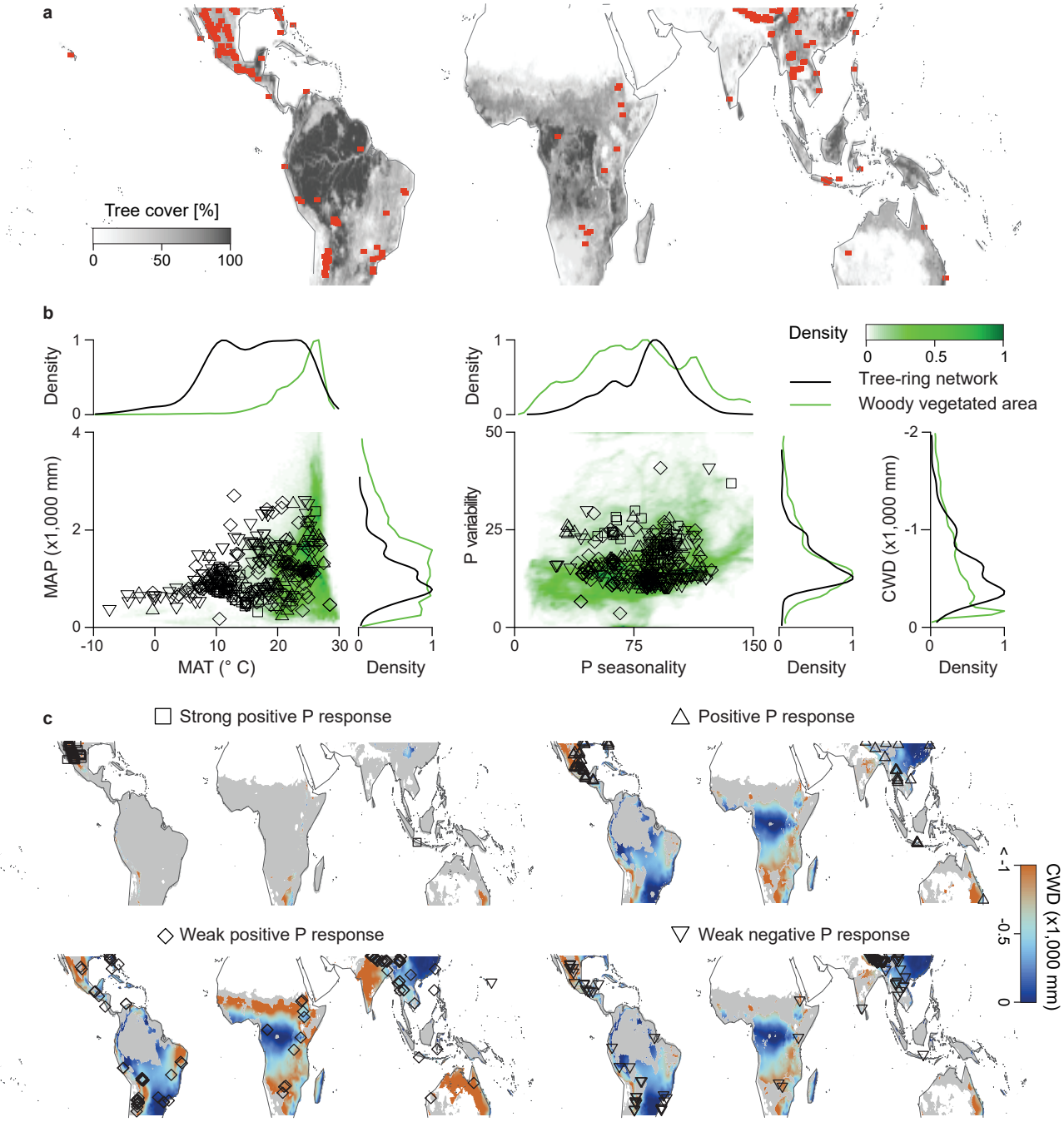
a
Tree cover [%]
0
50
100
b
Density
1
0
MAP (x1,000 mm)
4
2
0
-10
0
10
20
30
MAT (° C)
Density
0
1
P variability
50
25
0
75
150
P seasonality
CWD (x1,000 mm)
-2
-1
0
Density
0
0.5
1
Tree-ring network
Woody vegetated area
c
Strong positive P response
Positive P response
Weak positive P response
Weak negative P response
< -1
-0.5
0
CWD (x1,000 mm)

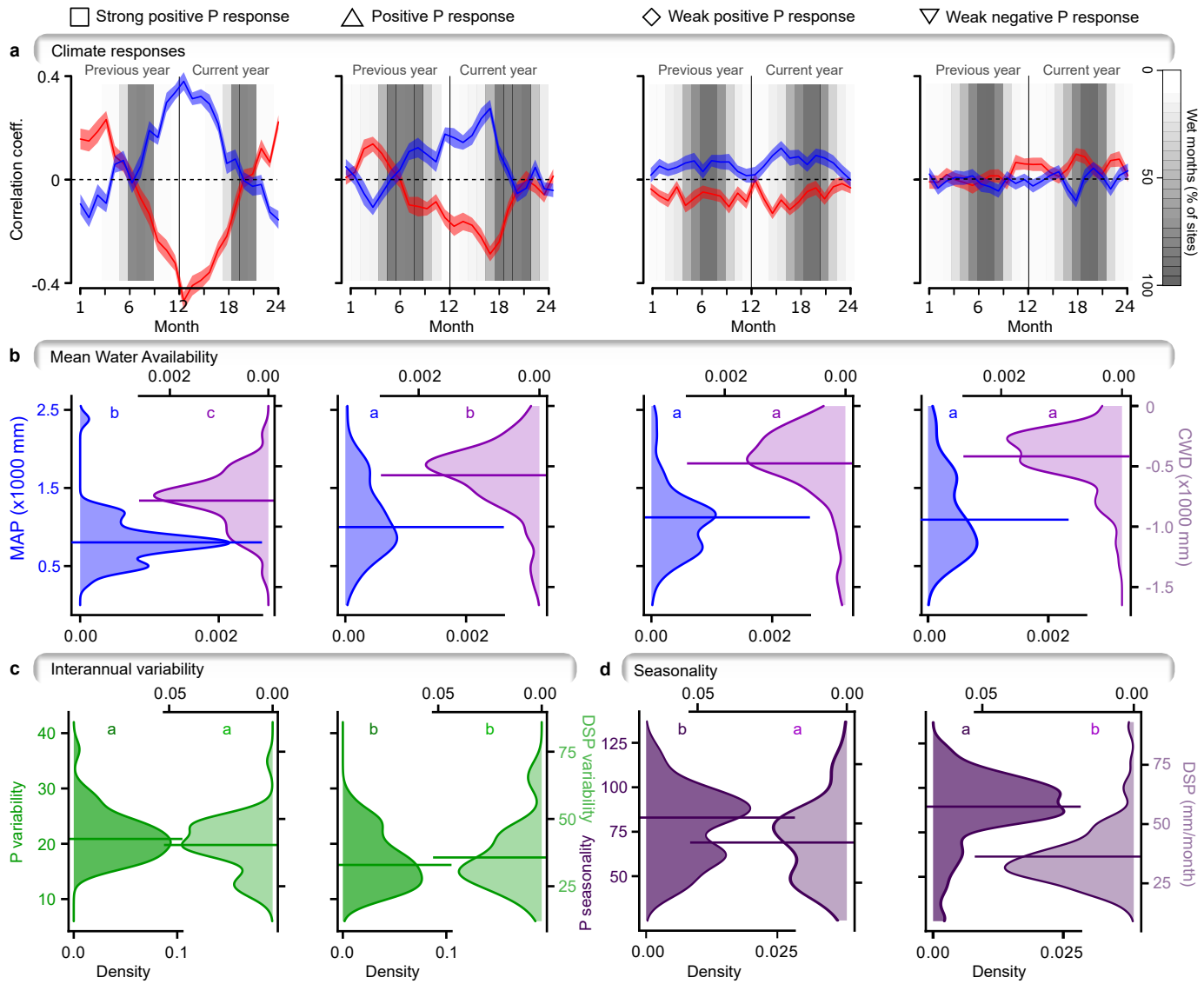
Strong positive P response
Positive P response
Weak positive P response
Weak negative P response
a
Climate responses
Previous year
Current year
Correlation coeff.
0.4
0
-0.4
1
6
12
18
24
Month
Wet months (% of sites)
0
50
100
b
Mean Water Availability
0.002
0.00
MAP (x1000 mm)
2.5
1.5
0.5
CWD (x1000 mm)
-0.5
-1.0
-1.5
c
Interannual variability
P variability
40
30
20
10
0.0
0.1
Density
DSP variability
P seasonality
75
50
25
d
Seasonality
125
100
75
50
0.025
DSP (mm/month)

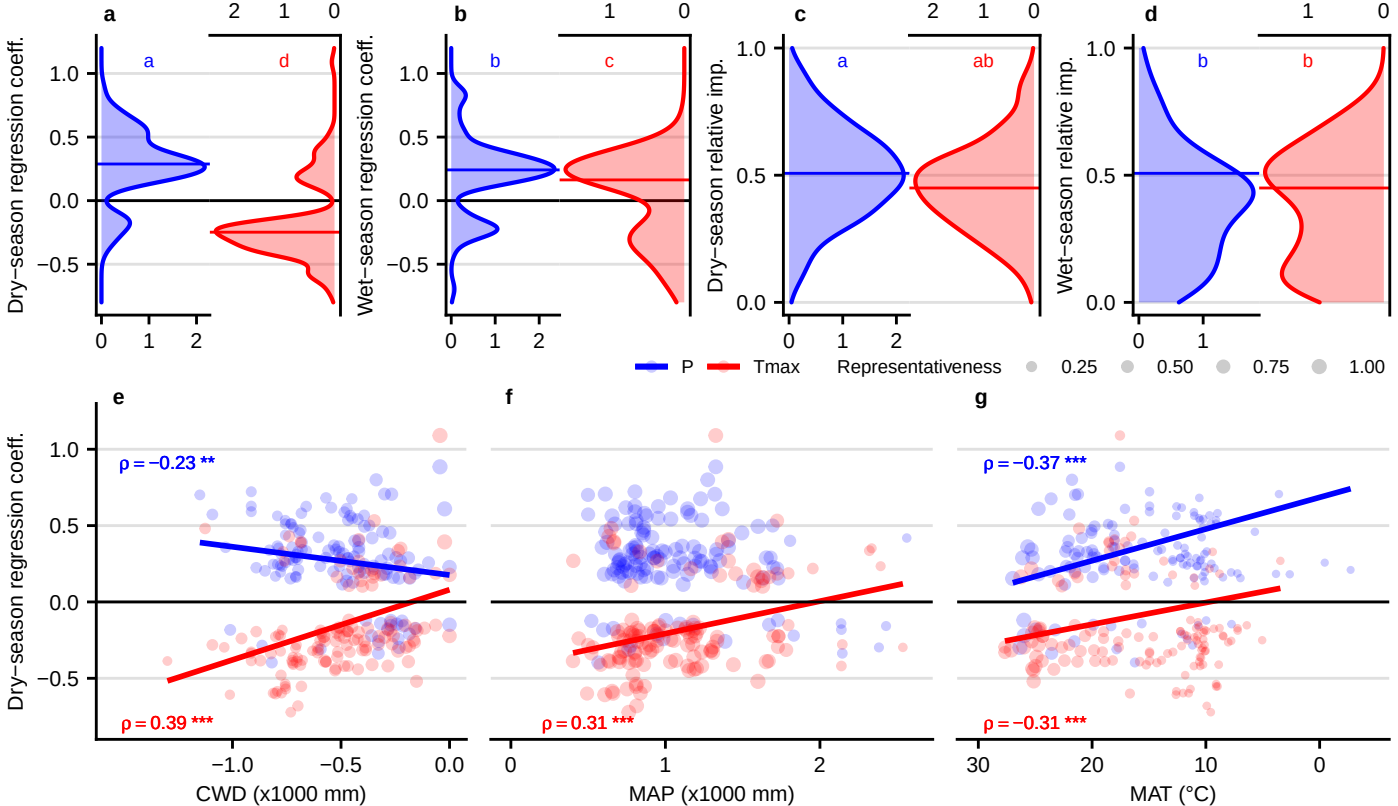
a
b
c
d
e
f
g
Dry−season regression coeff.
Wet−season regression coeff.
Dry−season relative imp.
Wet−season relative imp.
a
d
b
c
a
ab
b
b
P
Tmax
Representativeness
0.25
0.50
0.75
1.00
ρ = −0.23 **
ρ = 0.39 ***
ρ = 0.31 ***
ρ = −0.37 ***
ρ = −0.31 ***
CWD (x1000 mm)
MAP (x1000 mm)
MAT (°C)